

DOI: 10.1002/cctc.200((will be filled in by the editorial staff))

# CNT supported Mo<sub>x</sub>C catalysts: Impact of loading and carburization parameters

Benjamin Frank, Klaus Friedel, Frank Girgsdies, Xing Huang, Robert Schlögl, and Annette Trunschke\*

Mo<sub>x</sub>C/CNT catalysts were prepared by carburization of an oxidic Mo precursor impregnated on multiwalled carbon nanotubes (CNTs). The effects of different carburization atmospheres, heating rates, and Mo loadings were tested. The catalysts were characterized by CO-TPD, XRD, N<sub>2</sub> physisorption, SEM, and TEM. The catalytic performance in the steam reforming of methanol (SRM) was used as a sensitive probe to indicate changes in the catalyst surface during catalytic action. Contrarily to the bulk Mo<sub>x</sub>C catalysts the heating rate during carburization has practically no effect on the catalysts. Instead, Mo loading and carburization atmosphere are the key factors for catalyst

structure and performance. The Mo-based activity decreases at loadings >10 wt% at constant product selectivity. The CO<sub>2</sub>/CH<sub>4</sub> product ratio sensitively indicates changes in the catalyst properties at the loadings <20 wt%, where the activity is practically constant. Carburization in 20% CH<sub>4</sub>/H<sub>2</sub> yields 2 nm sized crystallites of cubic α-MoC. Carburization in pure H<sub>2</sub> and in He yields hexagonal β-Mo<sub>2</sub>C with a larger particle size. This phase change is documented in a different catalytic performance in terms of activity and CO<sub>2</sub>/CH<sub>4</sub> selectivity. Thus a multi-parameter toolbox for fine-tuning of catalyst properties is presented.

## Introduction

Group VI transition metal carbides provide catalytic features similar to expensive noble metals,<sup>[1]</sup> thus are permanently in the focus of intensive research. The high potential in reactions that involve the transfer of hydrogen, such as alkane (de)hydrogenations or isomerizations, ammonia decomposition, and Fischer-Tropsch synthesis has been documented.<sup>[2]</sup>

As the conventional metallurgical route to metal carbides typically provides very low specific surface areas (SSA), the first successful synthesis of high-surface area carbides by carburization of an oxidic precursor<sup>[3]</sup> was a break-through for catalytic application. However, the synthesis of porous carbides is demanding and it seems more appropriate to utilize a high surface area support such as alumina or carbon to stabilize highly dispersed carbide (nano)particles.<sup>[4–6]</sup> Carbon-based support materials can also serve as the carbon source for carburization. This economic strategy furthermore avoids the formation of passivating carbon deposits on the catalytically active carbide surface at the end of the carburization process, which easily occurs when using a gaseous hydrocarbon as the carbon source.

Few Mo<sub>x</sub>C/C catalysts have been reported in literature.<sup>[6–9]</sup> The carburization in CH<sub>4</sub>/H<sub>2</sub> mixtures typically leads to well dispersed Mo<sub>x</sub>C nanoparticles if the surface is sufficiently functionalized.<sup>[6,7]</sup> The synthesis of multiwalled CNT-supported β-Mo<sub>2</sub>C has been described by Bao *et al.*<sup>[6]</sup> They also highlighted the positive impact of nitric acid treatment of the CNT support prior to its impregnation with the Mo precursor. The abundance of surface oxygen groups created here enables a sufficient metal-support interaction to avoid agglomeration. However, a more systematic study on the influences of, e. g. Mo loading, carburization conditions, or specific surface properties, is still lacking. The variation of loading in a series of activated carbon and CNT supported Mo<sub>2</sub>C catalysts has been performed by

Solymosi *et al.*<sup>[10]</sup> During ethanol decomposition at 723 K the catalysts initially deactivate within the first 7 h time-on-stream. Unfortunately, neither steady state data nor different space velocities are reported to compare the patterns of product selectivities at a similar level of ethanol conversion. Furthermore, the study misses substantial parts of physico-chemical characterization of the samples, thus published data are difficult to interpret and do not support a structure-reactivity-correlation with regard to a catalyst optimization. However, a Mo loading in the range up to 17 wt%, depending on SSA of the support, has been shown to yield finely dispersed β-Mo<sub>2</sub>C nanoparticles. This is in good agreement with theoretical considerations: At optimum (maximum) loading the good wetting ability of MoO<sub>3</sub><sup>[11]</sup> would ideally lead to a homogeneous monolayer coverage of ~5.0 atoms Mo per square nanometer<sup>[12]</sup> as the prerequisite for finely dispersed carbide particles. Given a SSA of 300 m<sup>2</sup> g<sup>-1</sup> of a carbon support material this corresponds to a Mo<sub>x</sub>C loading of approx. 20 wt%.

The carburization conditions are predominantly discussed for bulk carbides.<sup>[13]</sup> Here a comparison of CH<sub>4</sub>/H<sub>2</sub> and C<sub>2</sub>H<sub>6</sub>/H<sub>2</sub> atmospheres shows that the formation of the carbide phase occurs slower in the presence of CH<sub>4</sub>,<sup>[14]</sup> which is the most stable alkane. On the other hand, the higher alkanes tend to easily decompose and favour coke deposition as an overlayer on the carbide particles. In the same study, the variation of the heating rate during carburization reveals that the lower rates enable the

[a] Dr. B. Frank, K. Friedel, Dr. F. Girgsdies, X. Huang, Prof. Dr. R. Schlögl, Dr. A. Trunschke  
Department of Inorganic Chemistry  
Fritz Haber Institute of the Max Planck Society  
Faradayweg 4-6  
Fax: (+) 49 30 8413 4405  
E-mail: trunschke@fhi-berlin.mpg.de

Supporting information for this article is available on the WWW under <http://dx.doi.org/10.1002/cctc.200xxxxx>.

carbide formation process to occur at lower temperatures. It is discussed that soot deposit is the active form of carbon and that then an interfacial reaction sets in driving C into Mo, which could explain the kinetic control of carburization. For low-temperature carburization Mo bronzes are required as intermediates in the topotactic transformation. Such mechanism is of particular interest when using a carbon-based support material itself, such as CNTs. Unfortunately, Hanif *et al.* do not report surface areas in their study,<sup>[14]</sup> however, according to the lower concentration of the carburization by-product H<sub>2</sub>O, also a structural benefit is expected from low heating rates. The phenomenon of hydrothermal sintering is well known from the reduction process of Fe-based catalysts for ammonia synthesis.<sup>[15]</sup> Both, the lower heating rate and a higher space velocity of the CH<sub>4</sub>/H<sub>2</sub> flow effectively lower the H<sub>2</sub>O concentration and at least for the bulk systems a strong structural impact is reported for Mo<sub>x</sub>C and Mo<sub>x</sub>N systems.<sup>[16,17]</sup> However, also adverse effects are observed<sup>[18]</sup> pointing at the high complexity of involved topotactical transformations, which are not fully understood.

## Results and Discussion

### Standard parameters and general observations

The standard MoC/oCNT system serving as the reference during all the catalyst modifications performed is the medium-loaded 20MoC/oCNT carburized in CH<sub>4</sub>/H<sub>2</sub> at a heating rate of 5 K min<sup>-1</sup>. As described in the introduction, a high concentration of well dispersed Mo species is expected here. Numerous reports confirm the complete carburization of oxidic Mo precursors in this atmosphere at 700°C,<sup>[6,14,19]</sup> thus ramping has been stopped at this temperature.

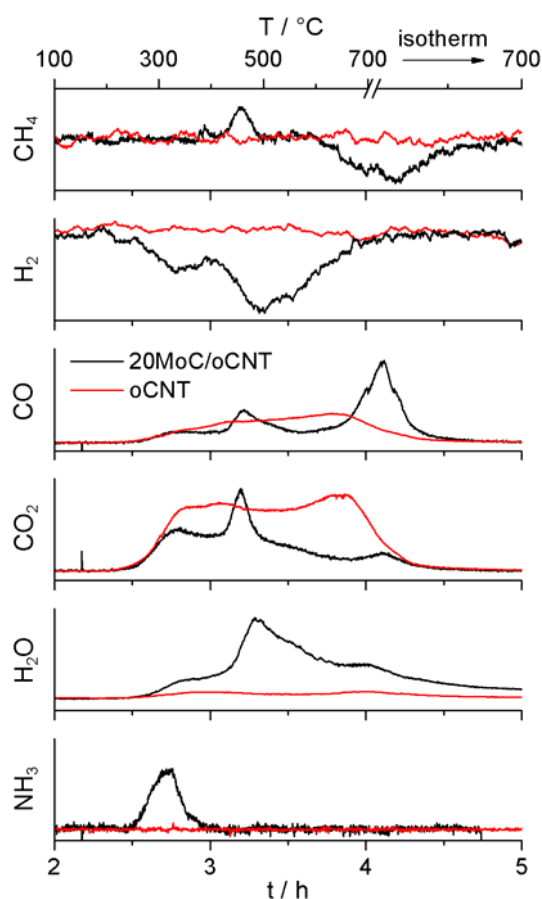


Figure 1. Profiles of CH<sub>4</sub> and H<sub>2</sub> consumption as well as of CO, CO<sub>2</sub>, H<sub>2</sub>O, and NH<sub>3</sub> formation during the carburization of 20MoC/oCNT and oCNT samples in 20% CH<sub>4</sub>/H<sub>2</sub> at 5 K min<sup>-1</sup> (after drying in CH<sub>4</sub>/H<sub>2</sub> at 100°C for 2 h). The profiles in arbitrary units are normalized with respect to the carbon mass of the sample.

The gases evolving during the carburization of 20MoC/oCNT are shown in Fig. 1. Due to the overlap with compounds being released from the metal-free oxidized carbon surface the blank oCNT is given as a reference. According to the traces of H<sub>2</sub> and CH<sub>4</sub> consumption as well as those of H<sub>2</sub>O, CO, and CO<sub>2</sub> formation the following transformations can be assigned to the features observed: (i) decomposition of the ammonium heptamolybdate (AHM) precursor into MoO<sub>3</sub>, (ii) reduction of MoO<sub>3</sub> to MoO<sub>2</sub>, (iii) partial carburization of MoO<sub>2</sub> into a non-stoichiometric oxycarbide MoO<sub>x</sub>C<sub>y</sub>, and (iv) complete carburization of MoO<sub>x</sub>C<sub>y</sub> into Mo<sub>x</sub>C. These steps are described extensively in literature,<sup>[6,14,19]</sup> where intermediate phases are identified by X-ray diffraction (XRD). In Fig. 1 step (i) can be located in the temperature range of 250–400°C, where the formation of NH<sub>3</sub> and H<sub>2</sub>O, respectively, is detected. H<sub>2</sub>O also evolves from the blank oCNT surface, however, to a much lesser extent than over the AHM loaded sample. The (partial) instantaneous reduction of Mo<sup>6+</sup> into Mo<sup>4+</sup> by H<sub>2</sub> is suggested by a weak drop of the H<sub>2</sub> profile, which is not observed for the oCNT sample. CO<sub>2</sub> and CO are massively released from the oxidized carbon surface due to the thermal decomposition of carboxylic acid and anhydride groups in this temperature range.<sup>[20]</sup> Step (ii) is the reduction of MoO<sub>3</sub> to MoO<sub>2</sub> at 400–500°C<sup>[14]</sup> by both H<sub>2</sub> and carbon atoms from the CNT surface. The first is supported by an enhanced H<sub>2</sub> consumption under H<sub>2</sub>O release; the latter is indicated by a sharp peak in both the CO and CO<sub>2</sub> profiles at 450°C, while no CH<sub>4</sub> is consumed here. Indeed, MoO<sub>3</sub> is well-known as a stoichiometric oxidant for elemental carbon.<sup>[21]</sup> Surprisingly, instead of CH<sub>4</sub> consumption a small amount of additional CH<sub>4</sub> is generated in the temperature range of step (ii), which is most likely due to the high CO<sub>x</sub> concentrations and the simultaneous presence of MoO<sub>2</sub> as a moderate CO<sub>x</sub> hydrogenation catalyst.<sup>[22]</sup> The intermediary formation of an orthorhombic Mo<sub>4</sub>O<sub>11</sub> phase is also suggested to occur in this temperature range.<sup>[13]</sup> The dissolution of support (CNT) carbon atoms into MoO<sub>x</sub> clusters, which points at defective carbon sites as the oxycarbide nucleation points, should also be considered.<sup>[23]</sup> Step (iii) covers the temperature range of 500–650°C and is indicated by still heavy, however, slowly declining consumption of H<sub>2</sub> under formation of H<sub>2</sub>O. Also the CO and CO<sub>2</sub> concentrations are still high, however, this is most likely caused by the steady defunctionalisation oCNT support.<sup>[20]</sup> The complete transformation into the oxycarbide MoO<sub>x</sub>C<sub>y</sub> is indicated by the finished H<sub>2</sub> consumption and the onset of CH<sub>4</sub> consumption. Finally, step (iv) is characterized by the heavy consumption of CH<sub>4</sub> under formation of CO, CO<sub>2</sub>, and H<sub>2</sub>O, which all slowly decay until the end of the carburization process after 1 h at 700°C.

It is noteworthy that the formation of CO and CO<sub>2</sub> from the blank oCNT sample temporarily exceeds their release from 20MoC/oCNT. This can be referred to the strong metal-support interaction between Mo species and the oxygen functionalities created on the carbon surface to anchor and disperse the AHM precursor as well as intermediate species. As suggested by Fig. 1, a substantial fraction of O atoms from the carbon surface are finally converted into H<sub>2</sub>O.

Temperature-programmed desorption (TPD) of CO was directly performed on the freshly carburized catalysts without exposition to ambient O<sub>2</sub> and H<sub>2</sub>O. Two main peaks at around 120 and a shoulder at 200°C are observed (Supporting Information, Fig. S1). The comparison with the blank oCNT material proves

that the CO profile exclusively originates from the interaction of CO with the Mo<sub>x</sub>C particles. In particular Yang *et al.* in their FTIR supported study of CO adsorption on MoN assigned peaks at similar positions to the desorption of CO from Mo<sup>δ+</sup> (0<δ<2) and N sites, respectively.<sup>[24]</sup> Due to the structurally and catalytically similar properties between Mo carbides and nitrides this assignment is tentatively adapted to Mo<sub>x</sub>C depending on the surface termination by Mo or by C (instead of N). Indeed, for β-Mo<sub>2</sub>C(0001) theory predicts quite similar stabilities of CO adsorbed on the top positions (t1) on C- and on Mo-terminated surfaces, respectively.<sup>[25]</sup> The total amount of CO desorbed up to 500°C is 332 μmol g(Mo<sub>x</sub>C)<sup>-1</sup>. This value appears rather low, however, it is reported that CO chemisorption on Mo<sub>x</sub>C at ambient temperature only measures ~14% of total adsorption sites.<sup>[26]</sup> Thus, the mean Mo<sub>x</sub>C particle diameter can be estimated as ~5 nm.<sup>[27]</sup>

Steam reforming of methanol (SRM) was chosen as a probe reaction due to a complex selectivity pattern, which is expected to sensitively indicate changes in the catalyst structure. In the reaction network of SRM, MeOH can react to CO<sub>2</sub> or CO,<sup>[28]</sup> which in the presence of H<sub>2</sub> can further react to CH<sub>4</sub> and higher alkanes/alkenes via Fischer Tropsch synthesis over Mo-based catalysts.<sup>[29]</sup>

The 20MoC/oCNT catalyst approaches a stable catalytic performance after 2 h time-on-stream at 250°C and only minor deactivation is observed in a 24 h test run. The conversion *X* of MeOH over this catalyst as a function of contact time is shown in the Supporting Information (Fig. S2a). The rapid increase in conversion is followed by a slow-down of the reaction rate after reaching approx. 50% conversion. This may be referred to inhibition by the main reaction products H<sub>2</sub> and CO<sub>2</sub> as observed over Cu-based catalysts,<sup>[30]</sup> although the overall reactant concentration is relatively low. The main carbon-based products of the reaction are CO<sub>2</sub> and CH<sub>4</sub>, whereas CO, C<sub>2</sub>H<sub>6</sub>, and C<sub>2</sub>H<sub>4</sub> are formed only in trace amounts. The following reactions are expected to predominantly contribute to the product pattern observed:

- (1) methanol steam reforming  
 $\text{CH}_3\text{OH} + \text{H}_2\text{O} \rightarrow \text{CO}_2 + 3 \text{H}_2$  ( $\Delta H^0 = 49.6 \text{ kJ mol}^{-1}$ )
- (2) methanol reduction  
 $\text{CH}_3\text{OH} + \text{H}_2 \rightarrow \text{CH}_4 + \text{H}_2\text{O}$  ( $\Delta H^0 = -115.4 \text{ kJ mol}^{-1}$ )
- (3) methanol decomposition  
 $\text{CH}_3\text{OH} \rightarrow \text{CO} + 2 \text{H}_2$  ( $\Delta H^0 = 90.6 \text{ kJ mol}^{-1}$ )
- (4) reverse water gas shift  
 $\text{CO}_2 + \text{H}_2 \rightarrow \text{CO} + \text{H}_2\text{O}$  ( $\Delta H^0 = 41.1 \text{ kJ mol}^{-1}$ )
- (5) CO<sub>x</sub> hydrogenation  
 $\text{CO}_x + \text{H}_2 \rightarrow \text{alkanes/alkenes} + \text{H}_2\text{O}$

In general, these observations agree with a previous report on supported Mo<sub>2</sub>C catalysts.<sup>[30,31]</sup> However, the detailed comparison of SRM activity fails due to different reaction conditions applied. The metal-free oCNT shows no catalytic activity under the reaction conditions applied.

Three parameters have been selected here to quantify changes in the catalytic performance of MoC/oCNT catalysts, namely the apparent activation energies of CO<sub>2</sub> and CH<sub>4</sub> formation, respectively, and the CO<sub>2</sub>/CH<sub>4</sub> product ratio (see Tab. 2). For 20MoC/oCNT carburized in CH<sub>4</sub>/H<sub>2</sub> at a heating rate of 5 K min<sup>-1</sup> the activation energies are 94 kJ mol<sup>-1</sup> and 108 kJ mol<sup>-1</sup>, respectively, and a product ratio of 4.1. The CO<sub>2</sub>/CH<sub>4</sub> ratio as a

function of MeOH conversion (see the Supporting Information, Fig. S2b) suggests that both CO<sub>2</sub> and CH<sub>4</sub> are primary products of the reaction; however, secondary methanation of CO<sub>2</sub> also occurs.

After SRM tests the catalyst samples were characterized by XRD, N<sub>2</sub>-physisorption, and electron microscopy. Due to the contact with H<sub>2</sub>O and CO<sub>2</sub> acting as mildly oxidizing agents<sup>[33]</sup> during SRM no surface passivation by low-concentrated O<sub>2</sub> was needed prior to exposition to ambient conditions. XRD confirms the pervasive transformation of AHM into face-centered cubic (fcc) α-MoC (Supporting Information, Fig. S3a). Although the catalyst has been used in a catalytic reaction involving potential oxidants such as H<sub>2</sub>O or CO<sub>2</sub> and even after long-term exposition to ambient conditions the patterns give no rise to oxidic bulk phases. As a reference, the pattern of molybdenum oxycarbide MoOC is characterized by a shift of the fcc pattern to higher angles,<sup>[34]</sup> which is indicative for a lattice contraction as a result of partial C-O-substitution. This is not the case here, where the detected peaks fall in line with the reference pattern for α-MoC.<sup>[35]</sup> Peak analysis reveals a crystallite size of approx. 2 nm. The reason for the formation of the metastable<sup>[35,36]</sup> fcc α-MoC instead of hexagonal close packed (hcp) β-Mo<sub>2</sub>C, which is predominantly reported to form under the synthesis conditions applied,<sup>[3,4,6,13,14,32]</sup> is not fully understood. Initially formed nuclei of sub-carbides or α-MoC may be formed at low temperatures, where the thermodynamic equilibration of the phases is inhibited for diffusion limitation, and prevail during synthesis. This is evidenced by the pronounced polycrystallinity of the material as described later. Han *et al.* suggest that the Mo<sub>x</sub>C phase can be controlled over the Mo loading on an ordered mesoporous carbon (OMC) support.<sup>[8]</sup> However, presented XRD diffractograms are difficult to interpret. It is more likely that the controlled reduction of the Mo precursor is the key factor for α-MoC synthesis. This has been successfully managed by MoO<sub>3</sub> pre-reduction in a H<sub>2</sub>/*n*-butane mixture,<sup>[37]</sup> or by adding 0.5% Pt to the Mo precursor to facilitate H<sub>2</sub> activation.<sup>[38]</sup> α-MoC proved a different performance than β-Mo<sub>2</sub>C in some catalytic reactions<sup>[9,36,38]</sup> and is traditionally prepared via nitridation of MoO<sub>3</sub> with NH<sub>3</sub> to fcc γ-Mo<sub>2</sub>N followed by subsequent re-carburization with CH<sub>4</sub>, which is a time- and resource-demanding process.<sup>[38]</sup> In this context the one-step preparation of CNT-supported α-MoC is a valuable observation.

The specific surface area of the catalyst drops from 290 to 163 m<sup>2</sup> g<sup>-1</sup> if compared to the metal-free oCNT (Tab. 1). This is most likely caused by plugging of open CNT tips by agglomerates of α-MoC. The XRD observations are in good agreement with the α-MoC particle size that is estimated by CO TPD.

### Impact of the heating rate during carburization

It is reported that the heating rate during the carburization of the metal carbide precursor can control the phase transformation temperatures and the pore structure of the resulting (bulk) carbide. Both effects are discussed for CNT supported systems at a nominal Mo<sub>x</sub>C loading of 20 wt%. The heating rates were varied in the range of 0.2 to 10 K min<sup>-1</sup>. For comparison the profiles of H<sub>2</sub>O evolution are assembled in Fig. 2.

Fig. 2 reveals a dramatic impact of the heating rate on the carburization process. If referred to the temperature, peaks are sharp and well resolved at the lowest heating rate of 0.2 K min<sup>-1</sup>. Here, the reaction is completed at approx. 600°C, however, on the cost of a reaction time of almost 50 h. Contrarily, at the highest heating rate of 10 K min<sup>-1</sup> peaks are broad and superimposed by each other. The release of H<sub>2</sub>O approaches zero not before 1 h heat treatment in the CH<sub>4</sub>/H<sub>2</sub> atmosphere. Nevertheless all the features observed at 0.2 K min<sup>-1</sup> can also be identified

here, indicating the successful carburization via the same intermediate phases in all the experiments.

The CO TPD (Supporting Information, Fig. S1) reveals no substantial differences between the 20MoC/oCNT samples carburized at different heating rates. The high-temperature shoulder is slightly more intense for the sample carburized at 1 K min<sup>-1</sup>. The amount of CO desorbed up to 500°C varies in the range of 330–380 μmol g(Mo<sub>x</sub>C)<sup>-1</sup> (Tab. 1) corresponding to a Mo<sub>x</sub>C particle size of 4–5 nm. Also the specific surface areas of the samples are very similar with a very weak tendency to the higher values at the lower heating rates. Partial methanation of the carbon support<sup>[40]</sup> to create a more defective surface or improved spreading of the Mo precursor during the protracted carburization process<sup>[11]</sup> might be the reasons for this observation.

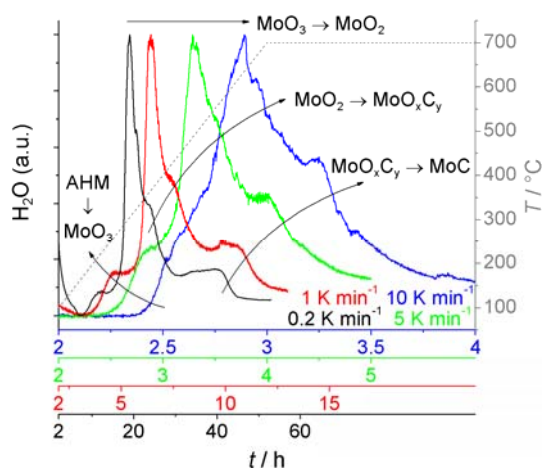


Figure 2. Profiles of H<sub>2</sub>O desorption during carburization of 20MoC/oCNT at different heating rates (after drying in CH<sub>4</sub>/H<sub>2</sub> at 100°C for 2 h). The m/e 18 traces are normalized for intensity and temperature

Table 1. Physico-chemical characterization of Mo <sub>x</sub> C/CNT catalysts				
Sample	β <sup>[a]</sup> / K min <sup>-1</sup>	Atmosphere	SSA / m <sup>2</sup> g <sup>-1</sup>	CO / μmol g(Mo <sub>x</sub> C) <sup>-1</sup>
oCNT	5	CH <sub>4</sub> /H <sub>2</sub>	290	0
20MoC/oCNT	0.2	CH <sub>4</sub> /H <sub>2</sub>	172	332
20MoC/oCNT	1	CH <sub>4</sub> /H <sub>2</sub>	169	379
20MoC/oCNT	5	CH <sub>4</sub> /H <sub>2</sub>	163	332
20MoC/oCNT	10	CH <sub>4</sub> /H <sub>2</sub>	163	346
5MoC/oCNT	5	CH <sub>4</sub> /H <sub>2</sub>	245	509
10MoC/oCNT	5	CH <sub>4</sub> /H <sub>2</sub>	197	391
30MoC/oCNT	5	CH <sub>4</sub> /H <sub>2</sub>	128	229
20MoC/oCNT	5	H <sub>2</sub>	170	143
20MoC/oCNT	5	He	146	66

[a] heating rate during carburization.

The similar catalytic performance in the SRM reaction (Supporting information, Tab. S1) suggests only minor differences in the catalyst structure according to the variation of the heating rate during carburization. The activities for methanol conversion

at 250°C are almost identical (Supporting information, Fig. S2a). The apparent activation energies of CO<sub>2</sub> and CH<sub>4</sub> formation appear unaffected in the ranges of 91–95 and 108 kJ mol<sup>-1</sup>, respectively. Accordingly, the CO<sub>2</sub>/CH<sub>4</sub> product ratio is fixed at around 4–5. The catalyst carburized at the lowest heating rate of 0.2 K min<sup>-1</sup> shows a weakly enhanced ratio of 5.1 (Supporting information, Fig. S2b), which is in agreement with a somewhat lower apparent activation energy of CO<sub>2</sub> formation.

Post-catalytic sample analysis by XRD reveals the presence of α-MoC nanocrystallites (~2 nm). The diffractograms are almost congruent (Supporting information, Fig. S3b) and free of reflexes other than α-MoC and graphitic CNTs. This finally proves that the heating rate during carburization in CH<sub>4</sub>/H<sub>2</sub> in the range of 0.2–10 K min<sup>-1</sup> has practically no effect on the structure and catalytic performance of 20MoC/oCNT catalysts. It is again worth mentioning that particles are polycrystals. These originate from frustrated growth at the mild conditions applied and this process is most likely induced by diffusion of defective carbon atoms from the support material into MoO<sub>x</sub> nuclei.<sup>[23]</sup> The formation of frustrated high-temperature metastable phases as active particles in turn might be the cause of activity and stability of the catalysts. Apparently, these can survive the redox stress during SRM much better than, e.g., single crystal surfaces or high-temperature phases converting into oxycarbides.

#### Variation of the metal loading of Mo<sub>x</sub>C/CNT catalysts

The metal loading of MoC/oCNT catalysts was varied between nominal Mo<sub>x</sub>C contents of 5–30 wt% to investigate the limits of surface coverage and agglomeration. AHM impregnated samples were carburized in CH<sub>4</sub>/H<sub>2</sub> at a heating rate of 5 K min<sup>-1</sup>.

The scanning electron microscopy (SEM) study reveals entangled CNTs without any agglomerates indicating the successful dispersion of metal species on the CNT surface. Even on the 30MoC/oCNT, which is the highest loading tested, bulky Mo<sub>x</sub>C particles cannot be visualized by SEM (Fig. 3a). The energy-dispersive analysis of X-ray (EDX) quantification of Mo and O confirms the nominal metal content and also indicates the presence of residual O on the surface of all samples (Fig. 3b). However, the O content is similar on all the catalysts and as high as on the blank oCNT sample, which similarly has been subjected to the carburization treatment and CO TPD, respectively. Thus, the O can likely be assigned to the metal-free fractions of the carbon surface. Especially the C-OH, C=O, and C-O-C groups formed during initial HNO<sub>3</sub> treatment are very stable,<sup>[20]</sup> thus can resist high temperatures in a reducing atmosphere.

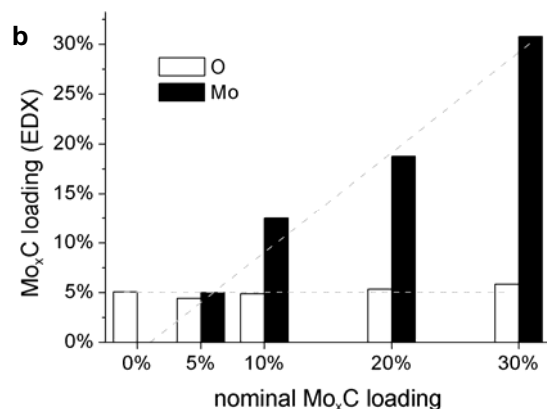
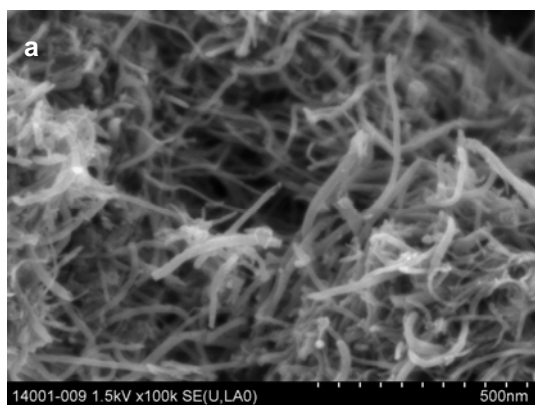


Figure 3. (a) Representative SEM image of 30MoC/oCNTs and (b) EDX analysis of MoC/oCNT catalysts. Dashed grey lines represent the parity line (Mo<sub>x</sub>C) and the average (O), respectively.

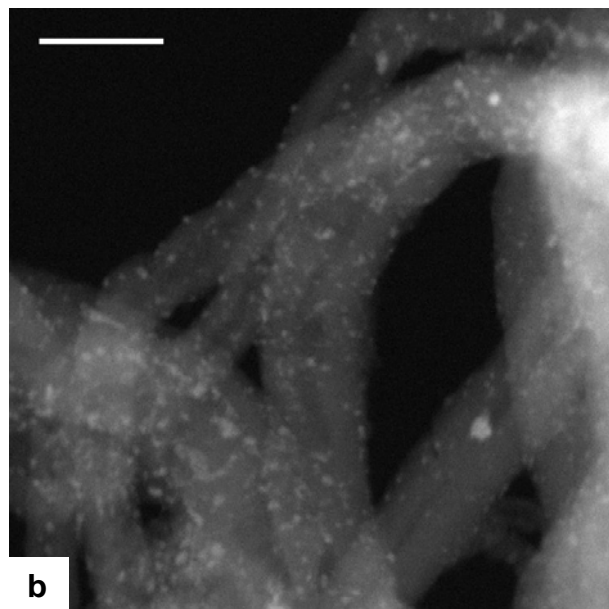
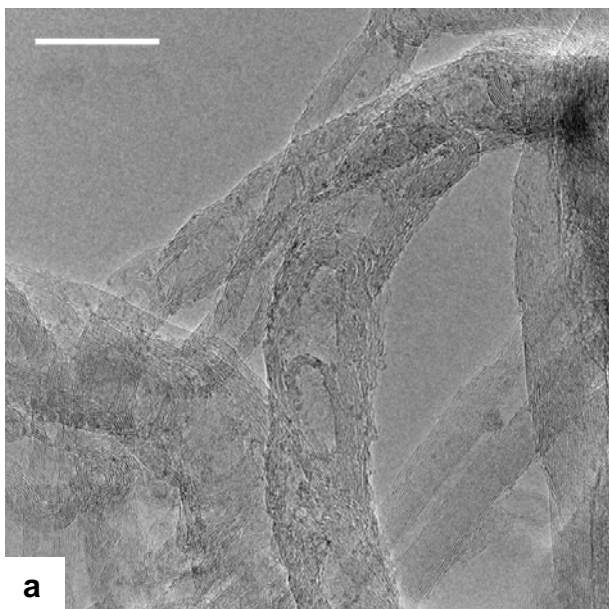


Figure 4. Representative (a) TEM and (b) corresponding HAADF images of the 5MoC/oCNT catalyst after reaction. Scalebar: 20 nm.

Transmission electron microscopy (TEM) gives an impression of the catalyst structure (Fig. 4a). The high dispersion of uniformly sized Mo<sub>x</sub>C particles is best seen in the scanning mode (STEM) at the lowest loading of 5 wt%. A representative high angle annular dark field (HAADF) image is shown in Fig. 4b. The mean particle size as estimated from these figures is 1–2 nm. At the higher loadings agglomeration of crystallites occurs (see the Supporting Information, Fig. S4). However, the still finely structured agglomerates of small (< 5 nm) α-MoC crystallites are located preferably at the outer CNT surface and at their tips, which were previously opened by harsh HNO<sub>3</sub> treatment. They vary in size but rarely exceed a diameter of 10 nm. It is also visible that the CNT structure is intact after the carburization process, which indicates that CH<sub>4</sub> rather than the support serves as the main carbon source for α-MoC formation.

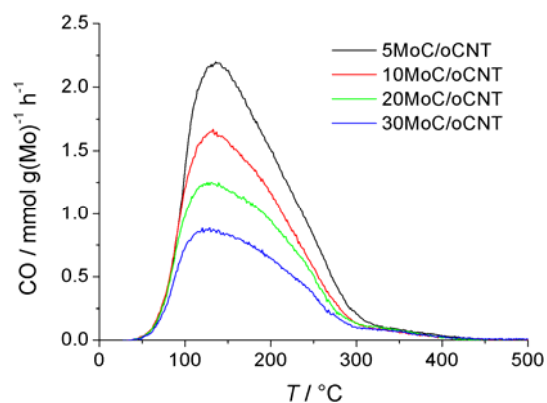


Figure 5. CO TPD profiles of differently loaded MoC/oCNT catalysts.

The quantitative analysis of CO TPD reveals a strong impact of the  $\text{Mo}_x\text{C}$  loading on the amount of CO desorbed at  $<500^\circ\text{C}$  (Fig. 5). If referred to the mass of  $\text{Mo}_x\text{C}$ , the low loaded 5MoC/oCNT catalyst provides more than twice as much adsorption sites than the highly loaded 30MoC/oCNT catalyst (Tab. 1). It indicates that the mean  $\text{Mo}_x\text{C}$  particle diameter within the MoC/oCNT loading series varies in the range of 3–7 nm. The detailed analysis of curve shapes in Fig. 5 points at two contributions, as discussed above, for all catalysts. For the loading series the high-temperature shoulder, which is assigned to the CO adsorption on C-terminated surface sites, is more pronounced at the higher loadings. In particular, the two-component Gaussian fit proves that the fraction of CO desorbed at  $\sim 200^\circ\text{C}$  steadily increases from 30 to 45% as the  $\text{Mo}_x\text{C}$  loading increases from 5 to 30 wt%. According to above assumptions this could be interpreted as an increased fraction of C-terminated  $\text{Mo}_x\text{C}$  surfaces with the increasing  $\text{Mo}_x\text{C}$  loading.

Regarding SRM catalysis two aspects have to be discussed. Firstly, the overall activity in terms of MeOH conversion (Fig. 6a) is similarly high for low loaded samples ( $\leq 10$  wt%  $\text{Mo}_x\text{C}$ ), if referred to the Mo content. The higher metal loadings decrease the effective reaction rate. Possible reasons are mass transport limitations in the high- $\text{Mo}_x\text{C}$  catalyst particles being too rich in active sites or larger  $\text{Mo}_x\text{C}$  particles having a lower specific (active) surface area. The results obtained from CO TPD suggest the latter although even at the low loadings the amount of CO adsorbed remarkably differs. The second aspect is the  $\text{CO}_2/\text{CH}_4$  product ratio (Fig. 6b). As listed in Tab. 2 the catalyst with the lowest  $\text{Mo}_x\text{C}$  loading of 5 wt% produces only half of the amount of  $\text{CH}_4$  that is produced over the highly loaded catalysts. The catalysts approach similar selectivities at  $\text{Mo}_x\text{C}$  loadings  $\geq 20$  wt%. The opposite trend has been reported for SRM over  $\text{Mo}_2\text{C}$  supported on active carbon.<sup>[31]</sup> Here, the  $\text{CO}_2/\text{CH}_4$  product ratios of 2.5 and 4.1 were measured at 50% MeOH conversion over 5 wt% and 10 wt% loaded  $\text{Mo}_2\text{C}/\text{C}$  catalysts, respectively. However, contrarily to the present study, high conversions have been achieved by temperature increase instead of GHSV variation. Thus, higher  $\text{CH}_4$  selectivities can also be a result of the reaction temperature. For 20MoC/oCNT this assumption is exemplarily confirmed by plotting the  $\text{CO}_2/\text{CH}_4$  ratio as a function of MeOH conversion during the step-wise temperature decrease from 250–200°C for determination of apparent activation energies (Supporting information, Fig. 2b). Indeed, the  $\text{CO}_2/\text{CH}_4$  ratio increases from 4.6 to 6.6 when lowering the temperature in this range, where the impact of conversion on  $\text{CO}_2/\text{CH}_4$  is rather low.

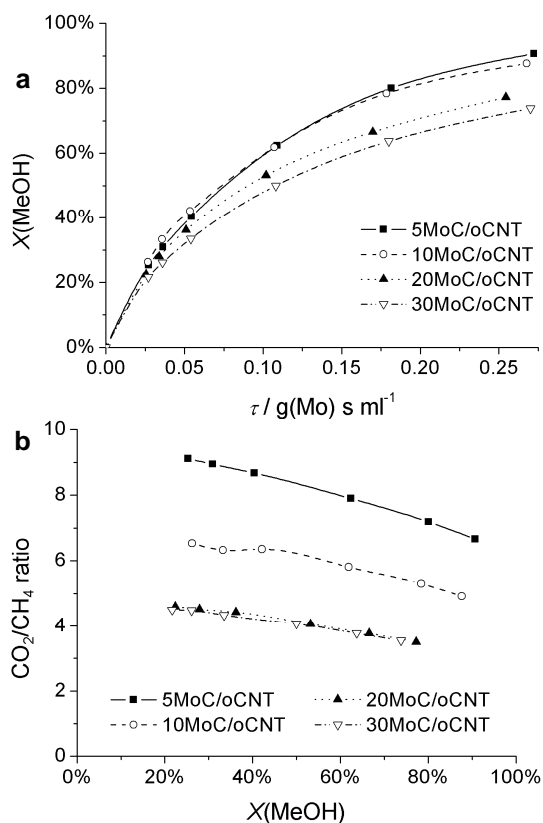


Figure 6. (a) Conversion of MeOH in the SRM reaction over MoC/oCNT catalysts as a function of the Mo-based contact time. (b)  $\text{CO}_2/\text{CH}_4$  product ratio as a function of MeOH conversion. Reaction conditions: 167–1000 mg catalyst, 10–100  $\text{ml min}^{-1}$  of 1% MeOH/1%  $\text{H}_2\text{O}/\text{He}$ ,  $250^\circ\text{C}$ .

**Table 2.** SRM performance data of MoC/oCNT catalysts with different loadings carburized at  $5 \text{ K min}^{-1}$  in  $\text{CH}_4/\text{H}_2$ .

Sample	$E_a(\text{CO}_2) / \text{kJ mol}^{-1}$	$E_a(\text{CH}_4) / \text{kJ mol}^{-1}$	$S(\text{CO}_2)/S(\text{CH}_4)^{[a]}$
oCNT	— <sup>[b]</sup>	— <sup>[b]</sup>	— <sup>[b]</sup>
5MoC/oCNT	95±1	111±1	8.4
10MoC/oCNT	93±2	111±1	6.1
15MoC/oCNT	91±1	108±1	4.0
20MoC/oCNT	94±2	108±2	4.1
30MoC/oCNT	92±2	108±1	4.1

[a]  $250^\circ\text{C}$ ,  $X(\text{MeOH})=50\%$ . [b] no catalytic activity observed.

The specific surface areas of the differently loaded catalysts decrease with the increasing Mo loading and finally approach  $128 \text{ m}^2 \text{ g}^{-1}$  (Tab. 1). It is well explained by the TEM observation of CNT open tips plugging with MoC. At the higher loadings also the mass fraction of MoC providing a lower SSA than the pure CNTs becomes a significant factor.

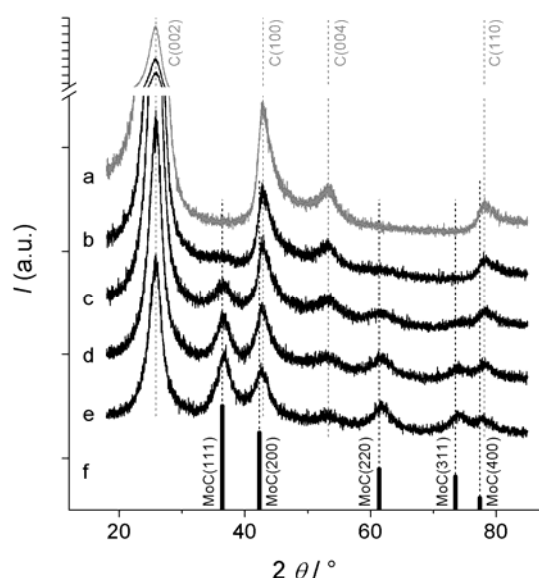


Figure 7. X-ray diffractograms of (a) oCNT and (b-e) Mo<sub>x</sub>C-loaded oCNT catalysts after catalytic reaction (top down: oCNT, 5MoC/oCNT, 10MoC/oCNT, 20MoC/oCNT, and 30MoC/oCNT); f) Reference pattern of  $\alpha$ -MoC.<sup>[34,40]</sup>

The X-ray diffractograms for the loading series are depicted in Fig. 7. The metal-free oCNT identifies the graphitic reflections originating from the support material. With the increasing Mo loading the pattern is supplemented by adding the reflections of fcc  $\alpha$ -MoC, which are clearly visible at a Mo<sub>x</sub>C loading of  $\geq 10$  wt%. A superposition appears at around 42–43° and at 77–78° with the MoC(200)/C(100) and MoC(400)/C(110) reflections, respectively. For all the samples with Mo<sub>x</sub>C  $\geq 10$  wt% the pattern analyses reveal an  $\alpha$ -MoC crystallite diameter of  $\sim 2$  nm.

### Influence of the carburization atmosphere

The carburization atmosphere can have significant influence on the Mo<sub>x</sub>C phase formed during carburization. Typically, in CH<sub>4</sub>/H<sub>2</sub> the hcp  $\beta$ -Mo<sub>2</sub>C is formed.<sup>[6]</sup> However, Han *et al.* show that the use of pure H<sub>2</sub> at 700°C leads to the formation of both  $\alpha$ -MoC and  $\beta$ -Mo<sub>2</sub>C depending on the Mo concentration on the OMC support,<sup>[6]</sup> which here serves as the carbon source. They also indicate that the carburization in inert N<sub>2</sub> at 700°C stops at the partially reduced MoO<sub>2</sub>. Similar carburization conditions are applied for 20MoC/oCNT catalysts.

The carburization profiles monitored in H<sub>2</sub> and in inert He atmospheres, respectively, are shown in Fig. 8. Similar to CH<sub>4</sub>/H<sub>2</sub> (Fig. 1), carburization starts with the decomposition of the AHM precursor under release of NH<sub>3</sub> and H<sub>2</sub>O at 250–350°C. However, for unknown reason less H<sub>2</sub>O is detected in H<sub>2</sub>. Here, a subsequent drop of the H<sub>2</sub> profile is seen, which is accompanied by steadily increasing H<sub>2</sub>O formation and indicates the reduction of MoO<sub>3</sub> into MoO<sub>2</sub> by H<sub>2</sub>. Carbon oxides are formed only to a relatively low extend. At 700°C, the formation of CH<sub>4</sub> is detected, which can originate from both, the methanation of released CO<sub>x</sub> and of the carbon support, respectively. Instead, when using He the formation of CH<sub>4</sub> is not observed and CO<sub>2</sub> and CO are the dominating gases produced, indicating that the reduction of Mo(VI) occurs via gasification of the carbon support.

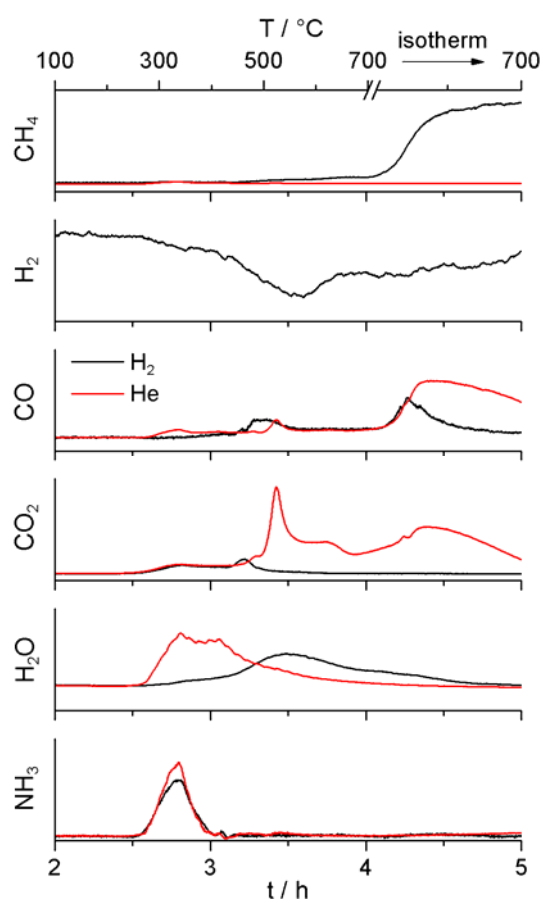


Figure 8. Profiles of H<sub>2</sub> consumption as well as of CH<sub>4</sub>, CO, CO<sub>2</sub>, H<sub>2</sub>O, and NH<sub>3</sub> formation during the carburization of 20MoC/oCNT in H<sub>2</sub> and in He at 5 K min<sup>-1</sup>, respectively.

The CO TPD experiments after carburization in H<sub>2</sub> and He show much less adsorption sites on the catalysts (Tab. 1, Fig. 9). This, however, originates from the mode of operation, i.e., the TPD starting at ambient temperature. Apparently, the profile is shifted to lower T upon alloying, making low-T desorption invisible in the set-up applied. Thus, the curves shown in Fig. 9 represent only the high-T shoulder of the whole profile. In particular, only 143 and 66  $\mu\text{mol g(Mo)}^{-1}$  can be detected, respectively, as compared to 332  $\mu\text{mol g(Mo)}^{-1}$  after carburization in CH<sub>4</sub>/H<sub>2</sub>. Again, two peaks are observed, however, the low-temperature contribution provides a much higher fraction of the overall profile. With regard to above assumptions it can be concluded that the only 25 and 20% of CO adsorption sites represent a C-termination of the Mo<sub>x</sub>C surface. This is plausible if we consider the hydrocarbon-free carburization atmosphere.

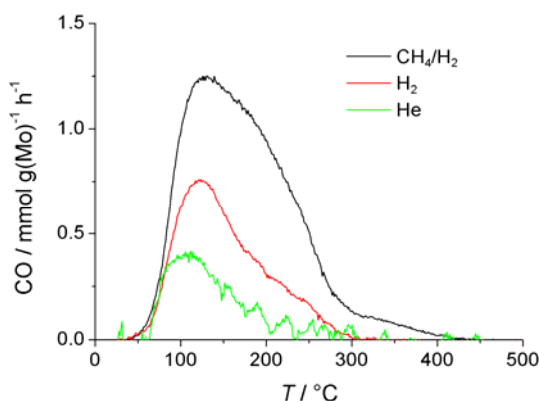


Figure 9. CO TPD profiles of 20 MoC/oCNT catalysts carburized in different atmospheres at 5 K min<sup>-1</sup>.

The catalytic performances also strongly depend on the carburization atmosphere. The catalyst carburized in pure H<sub>2</sub> is slightly more active than those carburized in CH<sub>4</sub>/H<sub>2</sub>. Instead, the carburization in inert He yields a poorly active catalyst. The microstructural changes are also reflected in the CO<sub>2</sub>/CH<sub>4</sub> product ratios. The catalytic data are assembled in Tab. 3 and in the Supporting Information, Fig. S5. The apparent activation energy of CO<sub>2</sub> formation drops to 87 and 88 kJ mol<sup>-1</sup> after carburization in H<sub>2</sub> and He, respectively, whereas the apparent activation energy of CH<sub>4</sub> formation changes to 105 and 128 kJ mol<sup>-1</sup>, respectively. Consequently, for both alternative carburization atmospheres the CO<sub>2</sub>/CH<sub>4</sub> product ratio remarkably increases and reaches a value as high as 9.2 after carburization in He.

**Table 3.** SRM performance data of 20MoC/oCNT catalysts carburized at 5 K min<sup>-1</sup> in different atmospheres.

Atmosphere	$E_{a,CO_2}$ / kJ mol <sup>-1</sup>	$E_{a,CH_4}$ / kJ mol <sup>-1</sup>	S(CO <sub>2</sub> )/S(CH <sub>4</sub> ) <sup>[a]</sup>
20% CH <sub>4</sub> /H <sub>2</sub>	94±2	108±2	4.1
H <sub>2</sub>	87±1	105±1	6.2
He	88±1	128±1	9.2

[a] 250°C, X(MeOH)=50%.

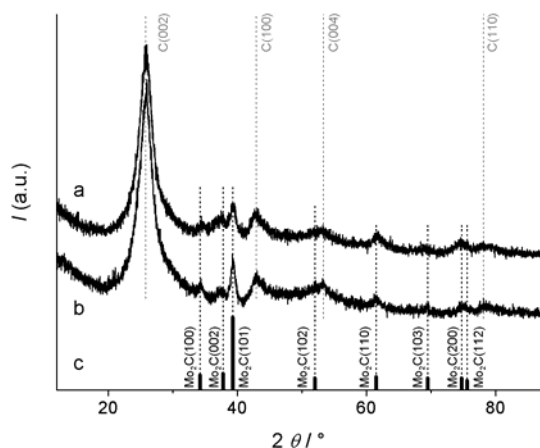


Figure 10. X-ray diffractograms of 20Mo/oCNT catalysts carburized (a) in H<sub>2</sub> and (b) in He after catalytic reaction; (c) Reference pattern of β-Mo<sub>2</sub>C.<sup>[40,41]</sup>

The reason for changes in the catalytic behaviour is poorly explained in the textural properties: catalysts carburized in H<sub>2</sub> and He provide specific surface areas of 170 and 146 m<sup>2</sup> g<sup>-1</sup>, which are quite close to the reference value of 163 m<sup>2</sup> g<sup>-1</sup> obtained by carburization in CH<sub>4</sub>/H<sub>2</sub> (Tab. 1). Besides CO TPD the most drastic change is seen in the XRD patterns of the catalysts (Fig. 10). Both the H<sub>2</sub> and He carburized samples show the typical bands of hcp β-Mo<sub>2</sub>C in addition to the pattern of graphitic CNTs. Its mean crystallite sizes are 8 and 10 nm after carburization in H<sub>2</sub> and He, respectively, which confirm the larger particle sizes estimated by CO TPD. Moreover, the H<sub>2</sub> carburized sample shows a band at ~38°, which could tentatively be interpreted as α-MoC or oxycarbide with a crystallite diameter of ~3 nm. If we consider the gases evolved during carburization, the formation of α-MoC on this sample could possibly be related with the presence of CH<sub>4</sub> at the end of the carburization process. Instead, on the He carburized sample a considerable amount of ~20% MoO<sub>2</sub> is detected (Fig. 10). Metallic Mo is identified on none of the XRD patterns.

The (partial) carburization of AHM in inert He at 700°C is a surprising result, as the temperatures required for such solid state reactions are typically much higher.<sup>[8,9]</sup> Taking the large crystallite size of remaining MoO<sub>2</sub> into account, the problem for incomplete reduction might be the Mo dispersion at elevated temperature. However, taking these differences in phase composition of the catalysts into account, the different catalytic performances (Tab. 3, Supporting information, Fig. S5) are not surprising. Results of the loading series and the variation of carburization atmosphere suggest that the formation of CO<sub>2</sub> and CH<sub>4</sub> could possibly be related with the Mo<sub>x</sub>C surface terminations by Mo and C, respectively.

## Conclusion

The preparation, characterization and catalytic testing of CNT-supported molybdenum carbide catalysts are presented. It is suggested that the nature of the Mo<sub>x</sub>C crystal phase is a sensitive function of the highly defective state of the CNT support structure, which kinetically controls the formation of favorable crystallization nuclei leading to a stabilized polycrystalline catalyst. The pervasive carburization can be controlled by the carburization atmosphere. The carburization at 700°C in CH<sub>4</sub>/H<sub>2</sub> yields α-MoC, whereas in pure H<sub>2</sub> a mixture of α-MoC and β-Mo<sub>2</sub>C is formed. In inert He only the β-Mo<sub>2</sub>C phase is formed, however, somewhat higher temperatures than 700°C are required according to the synthesis route applied in this study. The heating rate during carburization was found to be less important for the catalyst structure and reactivity. The Mo<sub>x</sub>C particle size as estimated by CO TPD steadily increases with the Mo<sub>x</sub>C loading from 5 to 30 wt%. Instead the crystallite size as given by XRD analysis remains constant at ~2 nm for α-MoC and <10 nm for β-Mo<sub>2</sub>C (note: volume-average). The CO TPD reveals two contributions, which are tentatively assigned to Mo and C terminated surfaces. According to this the fraction of C termination increases with the increasing Mo<sub>x</sub>C loading, however, sharply decreases when using a CH<sub>4</sub>-free carburization atmosphere.

The materials synthesized are highly active and stable catalysts in the SRM reaction. Here, the activity and product selectivity sensitively depend on the Mo<sub>x</sub>C loading and crystal phase. Probably also the surface termination by Mo or C plays an important role.

The experiments performed provide a versatile toolbox for the synthesis of differently performing catalysts, not only for SRM. It

is expected that trends and dependencies presented in this study to control the catalyst properties also provide important parameters to modify the activity and selectivity of CNT supported Mo<sub>x</sub>C catalysts in other reactions, e.g., the Fischer Tropsch alcohol synthesis. In this way the SRM reaction was applied rather as a probe reaction than as the economically/industrially highly interesting pathway for H<sub>2</sub> generation from liquid fuels.

## Experimental Section

**Synthesis:** Commercial MWCNTs (Baytubes C 150 HP) were pre-treated by refluxing in 65% HNO<sub>3</sub> (500 ml per 10 g) for 2 h. The product was washed with deionized water until neutral pH and dried in air at 110 °C for 1 day (oCNT). Aliquots of 1 g oCNT were impregnated with 3 ml of differently concentrated aqueous solutions of (NH<sub>4</sub>)<sub>6</sub>Mo<sub>7</sub>O<sub>24</sub>·4H<sub>2</sub>O, respectively, to achieve final Mo<sub>x</sub>C loadings between 5 and 30 wt%. Accordingly, samples are denoted as yMoC/oCNT, where y represents the nominal loading of Mo<sub>x</sub>C in wt%.<sup>[43]</sup> The resulting pastes were thoroughly kneaded in a mortar followed by drying in air at 110°C for 1 day. In a typical carburization procedure, a catalyst mass nominally containing 0.5 mmol Mo, e.g., 250 mg 20MoC/oCNT, was placed in a quartz tubular reactor (7 mm inner diameter) in a stream of 37 ml min<sup>-1</sup> of a 20 vol% CH<sub>4</sub>/H<sub>2</sub> mixture. After elution of H<sub>2</sub>O and O<sub>2</sub> (1 h at 100°C) the reactor temperature was linearly increased by 5 K min<sup>-1</sup> up to 700 °C and kept for 2 h, followed by cooling to ambient temperature in the reducing atmosphere.

**Characterization:** Temperature-programmed desorption (TPD) of CO was performed immediately after carburization without passivation or air contact of the catalyst. The reactor was flushed with 5 vol% CO/Ar for 10 min at ambient temperature and subsequently flushed with He until no CO was detectable by on-line mass spectrometry (MS, Pfeiffer GAM 200) and gas chromatography (GC, Varian xx Micro GC). In a He stream of 30 ml min<sup>-1</sup> the temperature was linearly increased by 10 K min<sup>-1</sup> up to 700 °C. Further characterization of the catalysts was performed after catalytic testing. Passivated samples were analyzed after exposition to ambient. TEM was performed on a FEI Cs-corrected Titan 80-300 microscope (300 kV) and SEM images were obtained on a Hitachi S-4800 FEG microscope (1.5 kV) equipped with an EDAX Genesis EDX detector (15 kV). The XRD measurements were performed on a Bruker AXS D8 Advance diffractometer equipped with a secondary graphite monochromator (Cu Kα<sub>1+2</sub> radiation) and scintillation detector. Crystallite size values were extracted by full pattern fitting and are reported as L<sub>Vol</sub>-IB values (volume weighted mean column length based on integral breadth) without further assumptions concerning crystallite shape or size distribution. N<sub>2</sub> physisorption was performed at 77 K in the relative pressure range of  $p/p_0 = 0.05-0.3$  after drying the sample in vacuum at 200°C for 2 h..

**Catalytic testing:** Catalysts were tested for their catalytic performance in the steam reforming of methanol (SRM) at 250 °C in 100 ml min<sup>-1</sup> of a 2 vol% CH<sub>3</sub>OH/2 vol% H<sub>2</sub>O/He mixture. After 2 h on stream, the flow rate was varied between 100 and 10 ml min<sup>-1</sup>, followed by decreasing the temperature in 10 K steps to 200 °C at 100 ml min<sup>-1</sup>. Reaction products were quantified by GC analysis. Contact of the catalyst with H<sub>2</sub>O (reactant) and CO<sub>2</sub> (product) ensured the mild passivation of the Mo<sub>x</sub>C surface, which is required prior to final exposure of the catalyst to ambient for its characterization.

## Acknowledgements

The authors thank W. Frandsen, F. Rybicki, G. Weinberg, and Z.-L. Xie for experimental assistance. Financial support by the

Federal Ministry of Education and Research (BMBF) within the CarboKat project (FKZ 03X0204C) of the Inno.CNT alliance is gratefully acknowledged.

**Keywords:** molybdenum carbide • crystal phase • surface termination • steam reforming of methanol • CO TPD

- [1] R. B. Levy, M. Boudart, *Science* **1973**, *181*, 547–549.
- [2] S. T. Oyama, in *Handbook of Heterogeneous Catalysis* (Eds.: G. Ertl, H. Knözinger, F. Schüth, J. Weitkamp), Wiley VCH, **2008**, pp. 342–356.
- [3] J. S. Lee, S. T. Oyama, M. Boudart, *J. Catal.* **1987**, *106*, 125–133.
- [4] A. J. Brungs, A. P. E. York, J. B. Claridge, C. Márquez-Alvarez, M. L. H. Green, *Catal. Lett.* **2000**, *70*, 117–122.
- [5] R. Barthos, A. Széchenyi, F. Solymosi, *Catal. Lett.* **2008**, *120*, 161–165.
- [6] X. Li, D. Ma, L. Chen, X. Bao, *Catal. Lett.* **2007**, *116*, 63–69.
- [7] C. Sayag, M. Benkhaleda, S. Suppanb, J. Trawczynskib, G. Djéga-Mariadassoua, *Appl. Catal. A* **2004**, *275*, 15–24.
- [8] J. Han, J. Duan, P. Chen, H. Lou, X. Zheng, H. Hong, *ChemSusChem* **2012**, *5*, 727–733.
- [9] H. Wang, A. Wang, X. Wang, T. Zhang, *Chem. Commun.* **2008**, 2565–2567.
- [10] R. Barthos, A. Széchenyi, Á. Koós, F. Solymosi, *Appl. Catal. A* **2007**, *327*, 95–105.
- [11] J. Haber, T. Machej, R. Grabowski, *Solid State Ionics* **1989**, *32–33, Part 2*, 887–892.
- [12] Y.-C. Xie, Y.-Q. Tang, in *Advances in Catalysis*, Academic Press, **1990**, pp. 1–43.
- [13] T. Cotter, The Reducibility of Mixed Mo/V Oxide Materials to Carbides and Their Reactivity in the Activation of Propane, Technische Universität Berlin, **2011**.
- [14] A. Hanif, T. Xiao, A. P. E. York, J. Sloan, M. L. H. Green, *Chem. Mater.* **2002**, *14*, 1009–1015.
- [15] R. Schlögl, in *Handbook of Heterogeneous Catalysis* (Eds.: G. Ertl, H. Knözinger, F. Schüth, J. Weitkamp), Wiley VCH, **2008**, pp. 2501–2575.
- [16] E. J. Markel, J. W. Van Zee, *J. Catal.* **1990**, *126*, 643–657.
- [17] C. H. Jagers, J. N. Michaels, A. M. Stacy, *Chem. Mater.* **1990**, *2*, 150–157.
- [18] J. G. Choi, J. R. Brenner, L. T. Thompson, *J. Catal.* **1995**, *154*, 33–40.
- [19] S. T. Oyama, J. C. Schlatter, J. E. Metcalfe, J. M. Lambert, *Ind. Eng. Chem. Res.* **1988**, *27*, 1639–1648.
- [20] J. L. Figueiredo, M. F. R. Pereira, *Catal. Today* **2010**, *150*, 2–7.
- [21] D. W. McKee, *Carbon* **1970**, *8*, 623–635.
- [22] J.-W. Dun, E. Gulari, B. Streusand, *Appl. Catal.* **1986**, *21*, 61–72.
- [23] A. Rinaldi, J.-P. Tessonnier, M. E. Schuster, R. Blume, F. Girgsdies, Q. Zhang, T. Jacob, S. B. Abd Hamid, D. S. Su, R. Schlögl, *Angew. Chem. Int. Ed.* **2011**, *50*, 3313–3317.
- [24] S. Yang, C. Li, J. Xu, Q. Xin, *J. Phys. Chem. B* **1998**, *102*, 6986–6993.
- [25] X.-R. Shi, J. Wang, K. Hermann, *J. Phys. Chem. C* **2010**, *114*, 13630–13641.
- [26] S. Ramanathan, S. T. Oyama, *J. Phys. Chem.* **1995**, *99*, 16365–16372.
- [27] Assumptions: spherical geometry, MoxC density = 8.2 g cm<sup>-3</sup>, CO site density 1015 cm<sup>-2</sup>, n.d.
- [28] Á. Mastalir, Á. Patzkó, B. Frank, R. Schomäcker, T. Ressler, R. Schlögl, *Catal. Commun.* **2007**, *8*, 1684–1690.
- [29] M. Saito, R. B. Anderson, *J. Catal.* **1980**, *63*, 438–446.
- [30] B. Frank, F. C. Jentoft, H. Soerijanto, J. Kröhnert, R. Schlögl, R. Schomäcker, *J. Catal.* **2007**, *246*, 177–192.
- [31] R. Barthos, F. Solymosi, *J. Catal.* **2007**, *249*, 289–299.
- [32] S. S.-Y. Lin, W. J. Thomson, T. J. Hagensen, S. Y. Ha, *Appl. Catal. A* **2007**, *318*, 121–127.
- [33] W. Wu, Z. Wu, C. Liang, P. Ying, Z. Feng, C. Li, *Phys. Chem. Chem. Phys.* **2004**, *6*, 5603.
- [34] I. F. Ferguson, J. B. Ainscough, D. Morse, A. W. Miller, *Nature* **1964**, *202*, 1327–1328.
- [35] O. Matsumoto, Y. Yaguchi, Y. Shiota, Y. Kanzaki, *High Temp. Sci.* **1983**, *16*, 243–250.
- [36] H. O. Pierson, in *Handbook of Refractory Carbides & Nitrides*, Noyes Publications, New Jersey, **1997**, pp. 110–112.
- [37] C. Bouchy, I. Schmidt, J. . Anderson, C. J. . Jacobsen, E. . Derouane, S. . Derouane-Abd Hamid, *J. Mol. Catal. A* **2000**, *163*, 283–296.
- [38] J. S. Lee, L. Volpe, F. H. Ribeiro, M. Boudart, *J. Catal.* **1988**, *112*, 44–53.
- [39] G. S. Ranhotra, A. T. Bell, J. A. Reimer, *J. Catal.* **1987**, *108*, 40–49.
- [40] J. Liu, J. Shen, X. Gao, L. Lin, *J. Therm. Anal. Calorim.* **1993**, *40*, 1245–1252.
- [41] Inorganic Crystal Structure Database, URL: <http://icsd.fkf.mpg.de/>, n.d.
- [42] E. Parthé, V. Sadogopan, *Acta Cryst.* **1963**, *16*, 202–205.
- [43] FHI internal sample numbers in parentheses: 05MoC/oCNT (13894); 10MoC/oCNT (13896); 20MoC/oCNT (13898 and 13899); 30MoC/oCNT (13901)

05MoC/oCNT (13894); 10MoC/oCNT (13896); 20MoC/oCNT (13898 and 13899); 30MoC/oCNT (13901).

---

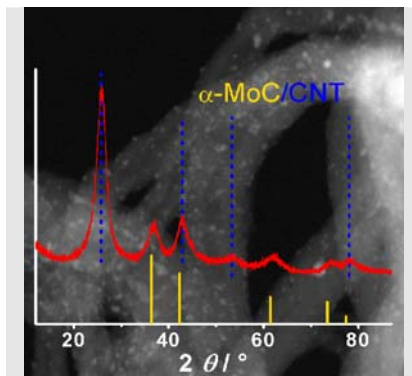
Received: ((will be filled in by the editorial staff))  
Published online: ((will be filled in by the editorial staff))

---

## Entry for the Table of Contents

### FULL PAPER

The synthesis of CNT-supported  $\alpha$ -MoC and  $\beta$ -Mo<sub>2</sub>C nanoparticles can be controlled by the carburization conditions applied. The impact of Mo loading, heating rate of carburization and carburization atmosphere as well as their impact on the catalytic performance of resulting Mo carbide catalysts in the steam reforming of methanol are discussed.



*Benjamin Frank, Klaus Friedel, Frank Girgsdies, Xing Huang, Robert Schlögl, and Annette Trunschke\**

**Page No. – Page No.**

**CNT supported Mo<sub>x</sub>C catalysts:  
Impact of loading and carburization  
parameters**

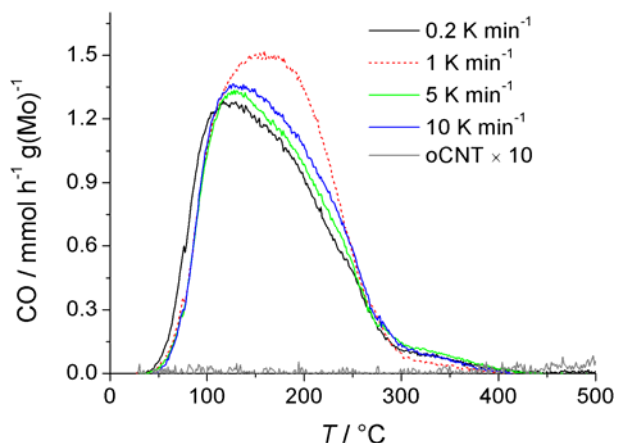


**Figure S1.** CO TPD profiles of 20MoC/oCNT catalysts ( $T$  ramping series). The increased intensity of the 1 K  $\text{min}^{-1}$  profile is most likely due to an experimental error.

$\beta$ / $\text{K min}^{-1}$	$E_a(\text{CO}_2)$ / $\text{kJ mol}^{-1}$	$E_a(\text{CH}_4)$ / $\text{kJ mol}^{-1}$	$S(\text{CO}_2)/S(\text{CH}_4)^{[a]}$
0.2	$91 \pm 3$	$108 \pm 1$	5.1
1	$95 \pm 1$	$108 \pm 1$	4.2
5	$94 \pm 2$	$108 \pm 2$	4.1
10	$92 \pm 2$	$108 \pm 1$	4.2

[a]  $250^\circ\text{C}$ ,  $X(\text{MeOH})=50\%$ .

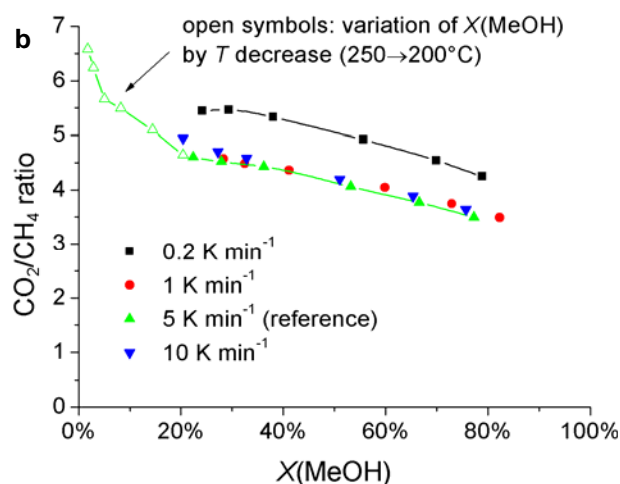
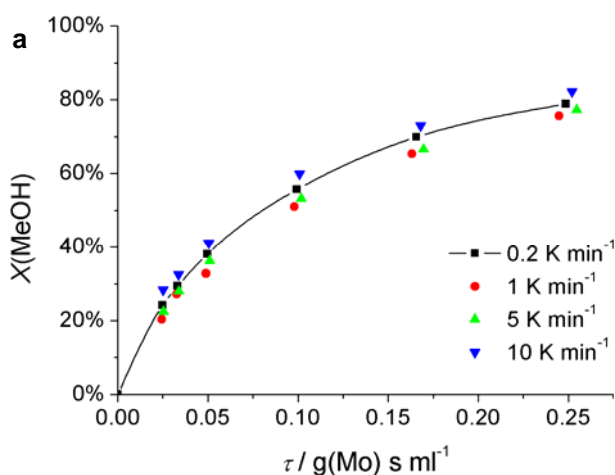


**Figure S2.** Catalytic performances of 20MoC/oCNT catalysts ( $T$  ramping series) in the SRM reaction. (a) MeOH conversion as a function of Mo-based contact time, (b)  $\text{CO}_2/\text{CH}_4$  product ratio as a function of MeOH conversion. 10-100  $\text{ml min}^{-1}$  1% MeOH/1%  $\text{H}_2\text{O}/\text{He}$ ,  $250^\circ\text{C}$ .

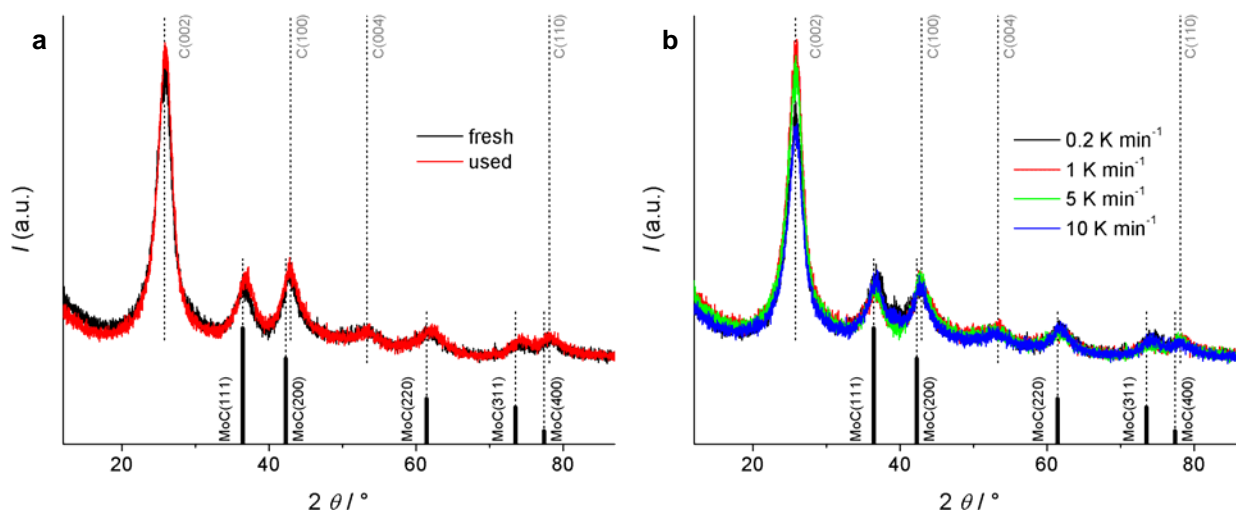


**Figure S3.** XRD patterns of 20MoC/oCNT catalysts (a) before and after catalytic reaction and (b) carburized at different heating rates in 20%  $\text{CH}_4/\text{H}_2$  (the fresh 20MoC-oCNT sample has the FHI internal sample number 13942).

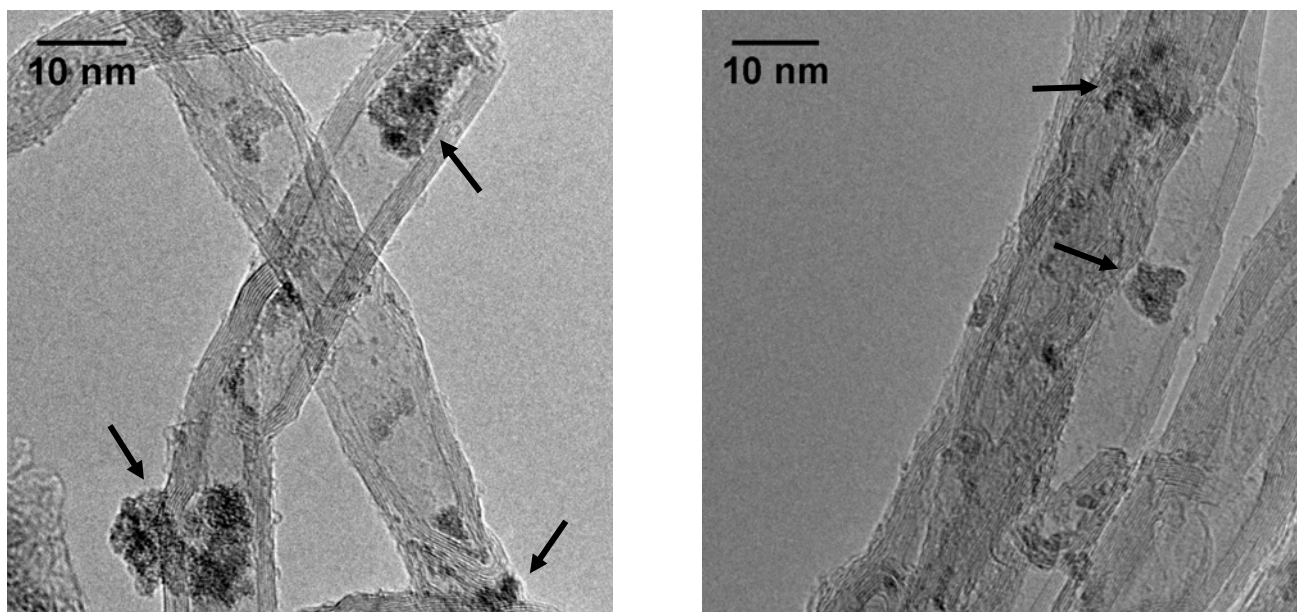


**Figure S4.** TEM images of high loaded 20MoC/oCNT catalyst showing agglomeration of Mo<sub>x</sub>C crystallites (arrows).

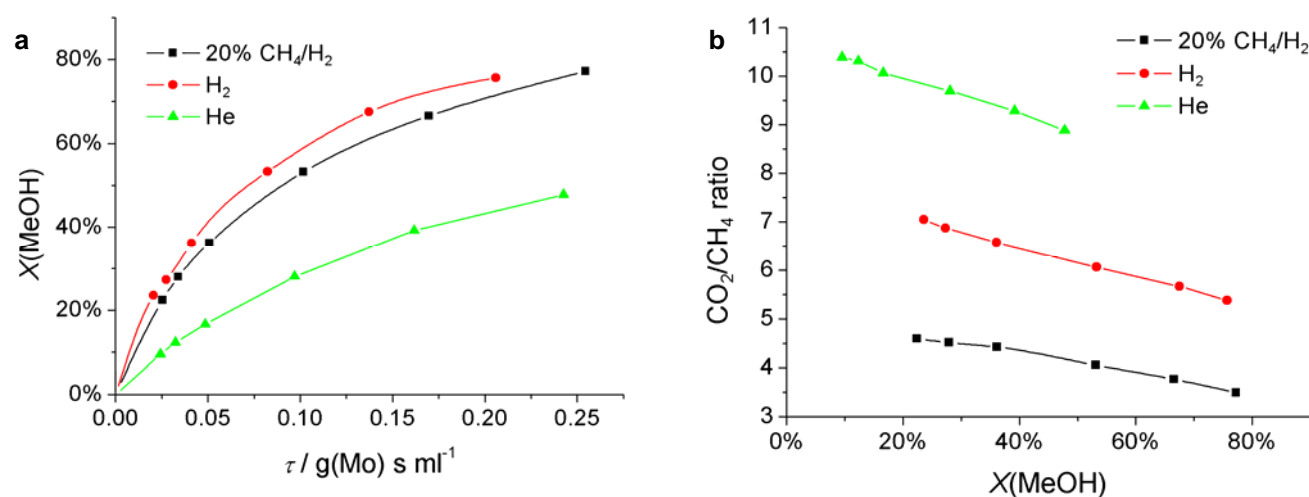


**Figure S5** Catalytic performances of 20MoC/oCNT catalysts (atmosphere series) in the SRM reaction. (a) MeOH conversion as a function of Mo-based contact time, (b) CO<sub>2</sub>/CH<sub>4</sub> product ratio as a function of MeOH conversion. 10-100 ml min<sup>-1</sup> 1% MeOH/1% H<sub>2</sub>O/He, 250°C.